Heriot-Watt University
Research Gateway

The Stiffening of Soft Soils on Railway Lines

Citation for published version:
Dong, K, Connolly, DP, Laghrouche, O, Woodward, PK & Alves Costa, P 2018, 'The Stiffening of Soft Soils on Railway Lines', *Transportation Geotechnics*, vol. 17, no. Part A, pp. 178-191. https://doi.org/10.1016/j.trgeo.2018.09.004

Digital Object Identifier (DOI):
10.1016/j.trgeo.2018.09.004

Link:
Link to publication record in Heriot-Watt Research Portal

Document Version:
Peer reviewed version

Published In:
Transportation Geotechnics

Publisher Rights Statement:
© 2018 Elsevier B.V.

General rights
Copyright for the publications made accessible via Heriot-Watt Research Portal is retained by the author(s) and / or other copyright owners and it is a condition of accessing these publications that users recognise and abide by the legal requirements associated with these rights.

Take down policy
Heriot-Watt University has made every reasonable effort to ensure that the content in Heriot-Watt Research Portal complies with UK legislation. If you believe that the public display of this file breaches copyright please contact open.access@hw.ac.uk providing details, and we will remove access to the work immediately and investigate your claim.

Download date: 25. Mar. 2025

Accepted Manuscript

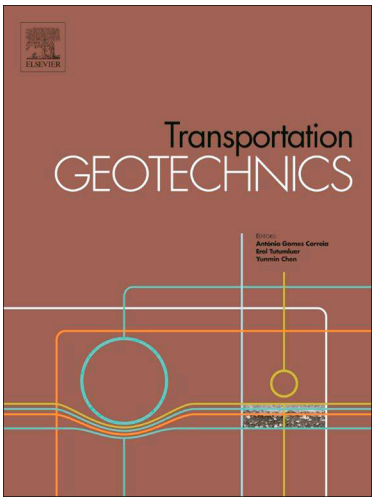

The Stiffening of Soft Soils on Railway Lines

K. Dong, D.P. Connolly, O. Laghrouche, P.K. Woodward, P. Alves Costa

PII: S2214-3912(18)30123-5
DOI: https://doi.org/10.1016/j.trgeo.2018.09.004
Reference: TRGEO 189

To appear in: *Transportation Geotechnics*

Received Date: 6 June 2018
Revised Date: 24 August 2018
Accepted Date: 10 September 2018

Please cite this article as: K. Dong, D.P. Connolly, O. Laghrouche, P.K. Woodward, P. Alves Costa, The Stiffening of Soft Soils on Railway Lines, *Transportation Geotechnics* (2018), doi: https://doi.org/10.1016/j.trgeo.2018.09.004

This is a PDF file of an unedited manuscript that has been accepted for publication. As a service to our customers we are providing this early version of the manuscript. The manuscript will undergo copyediting, typesetting, and review of the resulting proof before it is published in its final form. Please note that during the production process errors may be discovered which could affect the content, and all legal disclaimers that apply to the journal pertain.

ACCEPTED MANUSCRIPT

The author details are:

K. Dong: Heriot Watt University, EH14 4AS, UK.
D. P. Connolly, University of Leeds, LS2 9JT, UK.
O. Laghrouche: Heriot Watt University, EH14 4AS, UK.
P. K. Woodward, University of Leeds, LS2 9JT, UK.
P. Alves Costa, University of Porto, 4099-002 Porto, Portugal.

The Stiffening of Soft Soils on Railway Lines

Authors: K. Dong, D. P. Connolly, O. Laghrouche, P.K. Woodward, P. Alves Costa

Abstract

Railway tracks experience elevated rail deflections when the supporting soil is soft and/or the train speed is greater than approximately 50% of the wave propagation velocity in the track-soil system (i.e. the critical velocity). Such vibrations are undesirable, so soil replacement or soil improvement of the natural soil (or alternatively mini-piles or lime-cement treatment) is often used to increase track-ground stiffness prior to line construction. Although areas of existing soft subgrade might be easily identified on a potential new rail route, it is challenging to determine the type and depth of ground remediation required. Therefore, major cost savings can be made by optimising ground replacement/improvement strategies.

This paper presents a numerical railway model, designed for the dynamic analysis of track-ground vibrations induced by high speed rail lines. The model simulates the ground using a thin-layer finite element formulation capable of calculating 3D stresses and strains within the soil during train vehicle passage. The railroad track is modelled using a multi-layered formulation which permits wave propagation in the longitudinal direction, and is coupled with the soil model in the frequency-wavenumber domain. The model is validated using a combination of experimental railway field data, published numerical data and a commercial finite element package. It is shown to predict track and ground behaviour accurately for a range of train speeds.

The railway simulation model is computationally efficient and able to quickly assess dynamic, multi-layered soil response in the presence of ballast and slab track structures. Therefore it is well-suited to

ACCEPTED MANUSCRIPT

analysing the effect of different soil replacement strategies on dynamic track behaviour, which is particularly important when close to critical speed. To show this, three soil-embankment examples are used to compare the effect of different combinations of stiffness improvement (stiffness magnitude and remediation depths up to 5m) on track behaviour. It is found that improvement strategies must be carefully chosen depending upon the track type and existing subgrade layering configuration. Under certain circumstances, soil improvement can have a negligible effect, or possibly even result in elevated track vibration, which may increase long-term settlement. However, large benefits are possible, and if detailed analysis is performed, it is possible to minimise soil improvement depth with respect to construction cost.

Keywords: Railway ground improvement; railroad track stiffness; railway critical velocity; Rail-track dynamics Thin-layer method (TLM); subgrade soil replacement

1. Introduction

1.1 background

The global railway network is undergoing rapid expansion, with train vehicles becoming faster, heavier, and having less headway between successive passages. High axle freight loads are problematic on soft soil sites because they cause excessive track deflection. Similarly, faster trains are problematic because when the train speed exceeds approximately 50% of the natural ground wave speed, increases in track deflection occur. If deflections are high, it is a safety concern and results in more frequent maintenance due to accelerated track degradation. Therefore it is important to have a methodology capable of assessing remediation measures for both loading cases, ensuring track deflections meet desired tolerances.

The relationship between increases in track deflection and train speed is well documented (Zhai et al. 2010) and the speed at which maximum track displacement occurs due to a moving load is known as the 'critical velocity'. Although critical velocity effects (i.e. very high rail displacements) have been observed on numerous lines around the world , the most well documented case was at Ledsgard in Sweden (Madshus & Kaynia 2000)(Kaynia et al. 2000). At this site there were low stiffness soil layers resulting in a low site critical velocity. Therefore high track deflections were observed, particularly as train speed increased.

Ensuring soil stiffness' before the construction of a new line is constructed is challenging because soils are typically multi-layered and the dynamic behaviour of the track-soil system depends on multiple variables such as train speed. Therefore, on a new line there are 2 challenging scenarios which may be encountered after a critical velocity scoping study:

1. A low stiffness soil configuration which will likely require remediation (e.g. train speed > 70% of critical velocity)
2. A semi low stiffness soil configuration for which the need for remediation is unclear (e.g. train speed between 50-70% of critical velocity)

For both of these cases it is desirable to know how ground remediation will affect track behaviour. Two types of remediation often used on new lines are soil replacement and soil improvement (Steenbergen et al. 2007). These are potentially expensive and thus to minimise cost, analysis is required to determine the optimal depth and stiffness of the remediated ground.

The first step in analysing the potential for critical velocity effects to occur is to determine the site critical speed. For a homogenous soil this is straightforward, however in reality soils are multi-layered. Therefore an approach for solely calculating the critical velocity, rather than the track response was

ACCEPTED MANUSCRIPT

proposed by (Sheng et al. 2003)(Alves Costa, Colaço, Calçada, & Silva Cardoso, 2015)(Bian et al. 2016)(Mezher et al. 2016). These approaches relied on the analysis of the wave dispersion relationships in the track-ground system and found to give fast and reliable estimates of the critical velocity for layered soils.

In an attempt to simulate track dynamics at critical velocity, early researchers such as (Lamb 1904), (Fryba 1972) used analytical expressions to model the problem as a moving point load placed on an elastic half-space. Later, (Krylov 1995) and (Dieterman & Metrikine 1996) used a moving load to represent a train wheel, analytical expressions for the track structure and Green's functions for the soil.

Expanding upon this to simulate more complex layered soil cases, (Kaynia et al. 2000) proposed a semi-analytical model for the prediction of ground response. An embankment was modelled using an infinite viscoelastic beam and Green's function used to calculate the ground stiffness matrix. Further, (Sheng et al. 2003) and (Thompson 2008) proposed a semi-analytical approach in which the track was modelled analytically in the frequency domain and the soil was modelled using an integral transformation method. A similar approach was also followed by (Alves Costa, Calcada, et al. 2010)(Alves Costa 2011). The model was found to have agreement with field data collected at Ledsgard, Sweden.

Although analytical approaches are computationally efficient thus allowing for sensitivity analyses, they typically rely on a variety of assumptions thus making them valid for only a subset of real-world situations (Hendry et al. 2010). Therefore, to analyse the dynamics of more complex track structures, three dimensional (3D) models have been proposed. These include (Hall 2003) who developed a 3D finite element track-soil model using ABAQUS, which was subject to moving point loads. Building upon this, (Connolly, Giannopoulos & Forde 2013)(Connolly, Giannopoulos, Fan, et al. 2013), (Shih et al. 2016), (Shih et al. 2017), (Powrie et al. 2007) and (Varandas et al. 2016) also suggested using 3D models. Further, (El Kacimi et al. 2013) proposed a Fortran based 3D FE code in the time domain, while (Galvín & Domínguez 2007) proposed a frequency domain solution. (Kouroussis et al. 2011) also suggested using sub-modelling, where a multibody vehicle model was considered and combined with a 3D ABAQUS ground model surrounded by infinite elements. (Auersch 2005) and (O'Brien & Rizos 2005) coupled a multi-body vehicle system with a 3D FEM-BEM model to simulate the vibrations induced by high speed rails.

A challenge however with fully 3D numerical modelling is that it is computationally demanding. Alternatively, to reduce analysis run times, researchers have proposed using the periodic nature of railway tracks to reduce the number of degrees of freedom (Chebli, Othman, et al. 2008)(Chebli, Clouteau, et al. 2008)(Ferreira & López-Pita 2015)(Arlaud et al. 2015)(Arlaud et al. 2016). To do so, the track-soil can be divided into thin 3D finite element slices, the periodic modes computed and the solution transferred to the space domain via the Floquet transform.

Alternatively, to further reduce computational requirements, 2.5D models can be used approximate a 3D domain, and only require a similar number of computations as a 2D problem. (Yang et al. 2003) proposed this type of finite element solution, with an infinite element absorbing boundary solution. Alternatively (Alves Costa, Calçada, et al. 2010)used an equivalent linear 2.5D FEM-IEM approach to study the effects of soil non-linearity on the dynamic response of high-speed lines. (Bian, Chen, & Hu, 2008)(Bian, Chao, Jin, & Chen, 2011) also combined a 2.5D finite element model with one-quarter car model to study the vibrations caused by vertical track irregularities. Alternatively, (François et al. 2010) and (Galvín et al. 2010) presented efficient approaches for coupling both 2.5D FEM and 2.5D BEM, where the irregular domain was modelled using 2.5D FEM and the ground modelled using 2.5D BEM. (Alves Costa et al. 2012) also proposed a numerical scheme, based on the coupling between 2.5D FEM-BEM, to obtain the track-ground response. The result was found to agree well with field data from a test site in Portugal.

ACCEPTED MANUSCRIPT

When the system is considered invariant in the horizontal direction, the dynamic response of the ground can be simulated using a combination of analytical equations, combined with finite elements for the non-invariant direction (i.e., the vertical direction). This approach is known as the Thin-Layer Method (TLM), where the medium is discretised into thin layers in just a single (vertical) direction. These elements are similar to traditional 1D finite elements, however the horizontal directions are solved analytically, thus allowing the solution to be computed in a fraction of the time required for a full 3D model. The development of the generalised TLM is described by (Kausel 1981),(Kausel & Roesset 1981), (Kausel 1986) and (Kausel 1994). It has been used for railway problems by (Bian & Chen 2006) to obtain the semi-analytical solution for three-dimensional layered ground responses due to harmonic moving loads. Building on this work, (Alves Costa, Calcada, et al. 2010)(Alves Costa 2011)(Bian et al., 2016) also combined thin-layered elements with a 2.5D finite element method to predict train induced vibrations.

This work builds upon the work of these previous researchers and combines a TLM ground model with analytical modelling of the track structure. This results in a method that requires low computational effort to calculate track and ground responses due to high speed trains. The model is validated numerically and experimentally, and then used to investigate the effect of soil replacement/improvement below railway lines.

2. Model description

The model is a semi-analytical approach to compute vertical track displacements and three dimensional soil stresses/strains. It comprises of two main components: 1) an analytical track model, and 2) a semi-analytical thin-layer method ground model. Both sub-models are solved in the frequency domain and coupling is performed in the wavenumber-frequency domain, using relaxed boundary conditions between the track and soil. This means that only the vertical components are used for coupling because the 1D track model and 3D soil model have a different number of degrees of freedom (Kaynia et al. 2000)(Montalbán et al. 2015) The advantage of this approach is that the deep-wave propagation generated near critical velocity can be simulated both accurately and efficiently.

2.1 Track model

The track model is modelled in the wavenumber-frequency domain as previously described in (Alves Costa 2011)(Alves Costa et al. 2015)(Mezher et al. 2016). Different formulations are used to describe the ballasted and concrete slab tracks respectively, both of which assume the track to be infinite in the direction of train passage.

Figure 1 illustrates the ballasted track model. It is composed of rail, railpad, sleeper and ballast components, with the properties of discrete elements (e.g. sleepers and railpads) distributed along its length. Equation 1 describes the formulation which permits 1D wave propagation, where: k_x is the Fourier images of coordinates x; m_r and m_s are the mass of rail per metre and the equivalent distributed mass of the sleepers respectively; k_p^* is the complex stiffness of the railpad, i.e, including damping ($k_p^* = k_p(1 + i\omega c_p)$), where $*$ indicates a complex number; C_p is the ballast compressional wave speed; E_b is the ballasts Young's modulus; h_b is the ballast height; $2b$ is the track width; $\tilde{u}_r$, $\tilde{u}_s$and $\tilde{u}_{bb}$ are the rail, sleeper, and ballast (bottom) displacements respectively ($\sim$ represents frequency domain response); P is the vertical force acting on the rail.

ACCEPTED MANUSCRIPT

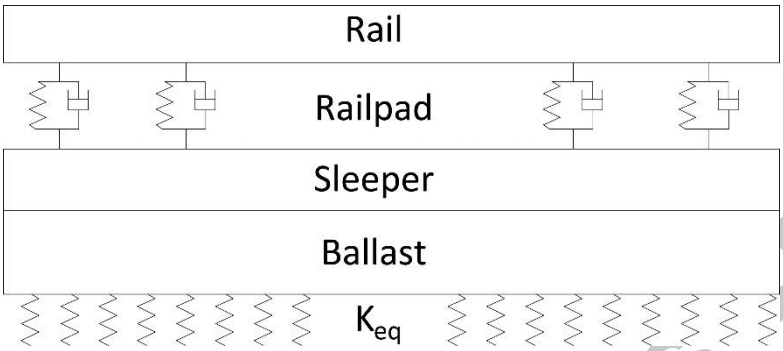

Figure 1: Ballasted track model structure

$$\begin{bmatrix} EI_r k_x^4 + k_p^* - \omega^2 m_r & -k_p^* & 0 \\ -k_p^* & k_p^* + \dfrac{2\omega E_b^* b\alpha}{\tan\left(\frac{\omega h_b}{C_p}\right) C_p} - \omega^2 m_s & \dfrac{-2\omega E_b^* b\alpha}{\sin\left(\frac{\omega h_b}{C_p}\right) C_p} \\ 0 & \dfrac{-2\omega E_b^* b\alpha}{\sin\left(\frac{\omega h_b}{C_p}\right) C_p} & \dfrac{2\omega E_b^* b\alpha}{\tan\left(\frac{\omega h_b}{C_p}\right) C_p} + k_{eq} \end{bmatrix} \begin{Bmatrix} \tilde{u}_r(k_x,\omega) \\ \tilde{u}_s(k_x,\omega) \\ \tilde{u}_{bb}(k_x,\omega) \end{Bmatrix} = \begin{Bmatrix} \tilde{P}(k_x,\omega) \\ 0 \\ 0 \end{Bmatrix} \quad (1)$$

Figure 2 illustrates the layout of the slab track model, which unlike the ballasted track, considers the bending stiffness of the concrete slab. The governing equations for the slab track are shown in Equation 2, where: EI_{sl} is the bending stiffness of the slab; m_{sl} is the mass of the slab per meter and $\tilde{u}_{sl}$ is the vertical slab displacement in the frequency domain.

ACCEPTED MANUSCRIPT

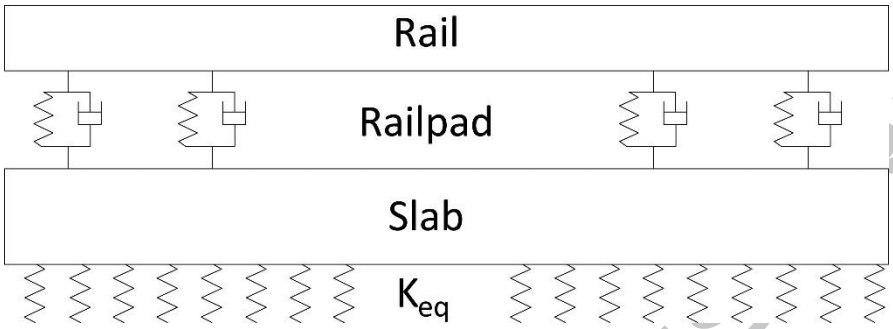

Figure 2: Slab track model structure

$$\begin{bmatrix} EI_r k_x^4 + k_p^* - \omega^2 m_r & -k_p^* \\ -k_p^* & EI_{sl} k_x^4 + k_p^* - \omega^2 m_{sl} + k_{eq} \end{bmatrix} \begin{Bmatrix} \tilde{u}_r(k_x, \omega) \\ \tilde{u}_{sl}(k_x, \omega) \end{Bmatrix} = \begin{Bmatrix} \tilde{P}(k_x, \omega) \\ 0 \end{Bmatrix} \quad (2)$$

For both track types, track-soil coupling is achieved using a complex equivalent stiffness (k_{eq}) defined in the wavenumber-frequency domain, as shown in Equation 3. Higher train speeds typically result in greater wave propagation across the track-soil interface. Therefore the accuracy of coupling across this interface is vital for reliable simulation. In this equation, $\tilde{u}_{zz}^G$ is the Green's function describing the vertical displacement of the surface of the ground, while k_x and k_y are the Fourier images of coordinates x and y respectively. For both tracks, coupling is achieved by taking into account the equilibrium of loads and the compatibility of displacements along the track-ground interface (Steenbergen & Metrikine 2007):

$$\tilde{k}_{eq}(k_x, \omega) = \frac{2\pi}{\int_{-\infty}^{+\infty} \tilde{u}_{zz}^G(k_x, k_y, z = 0, \omega) C_{tg} dk_y} \quad (3)$$

Where C_{tg} is a scaling factor for the track-ground coupling. For the case of a ballasted track, coupling is achieved through compatibility of displacements at the track centre point on the track-ground boundary:

$$C_{tg} = \frac{\sin(k_y b)}{k_y b} \quad (4)$$

Whereas for the slab track, coupling is achieved through compatibility of the average displacements across the track-ground boundary:

$$C_{tg} = \frac{\sin(k_y b)^2}{(k_y b)^2} \quad (5)$$

ACCEPTED MANUSCRIPT

For both track cases, relaxed boundary conditions are assumed, i.e., the compatibility and equilibrium conditions are only respected in the vertical direction. This is considered valid because vertical excitation is dominant during train passage.

2.2 Soil Model

2.2.1 Thin-layer method formulation

The thin-layer method (TLM) is a semi-analytical approach commonly used to solve wave propagation problems in 3D unbounded domains (e.g. soils). It relies on discretizing the vertical plane into a finite number of layers, each thin with respect to wavelength, meaning vertical displacements can be assumed to vary linearly across each layer. Regarding the horizontal directions, the analytical wave equation is used to rapidly calculate harmonic displacements without suffering from the element aspect-ratio restriction of the finite element method.

The thin layer formulation is undertaken in the frequency-wavenumber domain, with the response computed for each individual frequency under steady-state harmonic conditions. It allows the soil to be discretized along the z-direction with the infinite and homogeneous property along the horizontal plane, as shown in Figure 3, in which n represents the total number of vertically discretised soil layers. To ensure the propagation of stresses/strains inside the soil domain is modelled correctly, three-node quadratic thin-layer elements are used (Figure 4). Also, to ensure the thickness of each layer is small with respect to the wavelength, all thin layers meet the criteria outlined in Equation 6, where k_{max} is the maximum wavenumber under consideration.

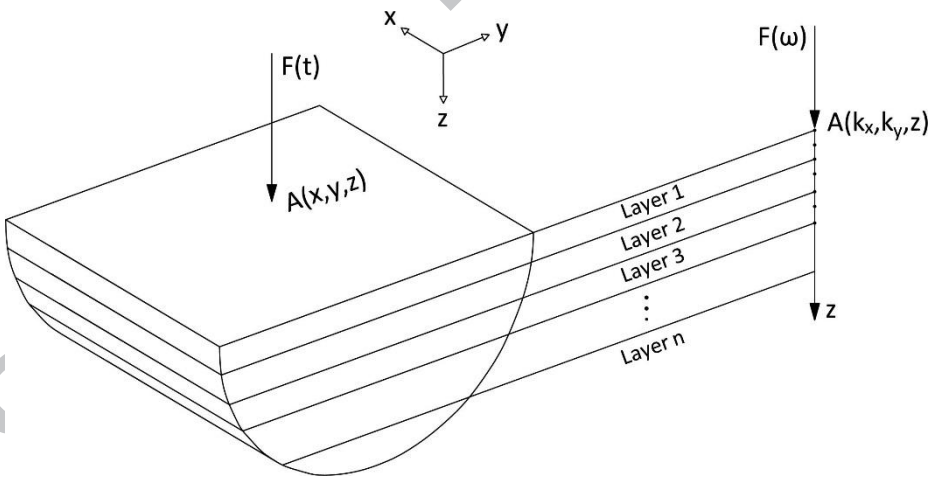

Figure 3: Schematic drawing of the procedure of the vertical discretization and domain transform in the thin-layer method

ACCEPTED MANUSCRIPT

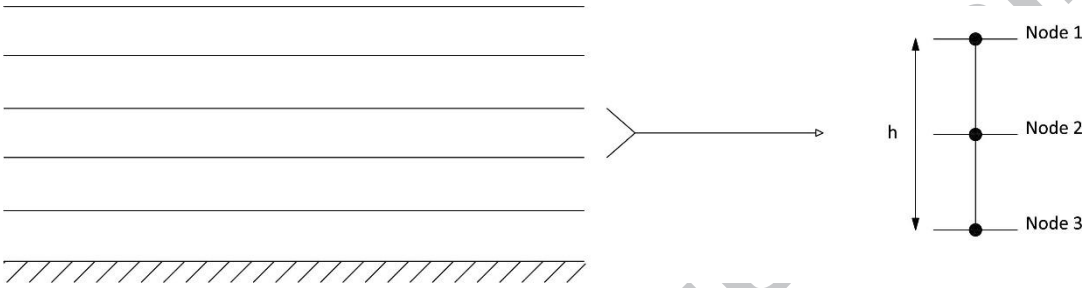

Figure 4: Discretization into thin layers with quadratic interpolation

$$h = \frac{wavelength}{8} = \frac{2\pi}{8k_{max}} \tag{6}$$

The displacement field inside each thin layer is approximated by means of the interpolation function (shape function), i.e., $\mathbf{u} = \mathbf{NU}$, where $\mathbf{U}$ is a vector containing the nodal displacements. Also, $\mathbf{N} = \mathbf{N}(\xi)$ is the shape function matrix of the form, $\mathbf{N} = [N_1\mathbf{I}\ N_2\mathbf{I}\ N_3\mathbf{I}]$ where N_a is the shape function and $\mathbf{I}$ the 3×3 identity matrix and ξ represents the local coordinates. For a three noded thin-layer element, the shape functions are:

$$N_1(\xi) = \frac{1}{2}\xi^2 - \frac{1}{2}\xi \tag{7}$$

$$N_2(\xi) = 1 - \xi^2 \tag{8}$$

$$N_3(\xi) = \frac{1}{2}\xi^2 + \frac{1}{2}\xi \tag{9}$$

Next, strains and stresses inside each layer are approximated as $\{\boldsymbol{\varepsilon}\} = [\mathbf{B}]\{\mathbf{U}\}$ and $\{\boldsymbol{\sigma}\} = [\mathbf{D}]\{\boldsymbol{\varepsilon}\} = [\mathbf{D}][\mathbf{B}]\{\mathbf{U}\}$, where $[\mathbf{B}]$ is the strain matrix and $[\mathbf{B}] = [\mathbf{B_1} \quad \mathbf{B_2} \quad \mathbf{B_3}]$ and

ACCEPTED MANUSCRIPT

$$[\mathbf{B}_a] = \begin{pmatrix} ik_x N_a & 0 & 0 \\ 0 & ik_y N_a & 0 \\ 0 & 0 & \frac{\partial N_a}{\partial z} \\ ik_y N_a & ik_x N_a & 0 \\ 0 & \frac{\partial N_a}{\partial z} & ik_y N_a \\ \frac{\partial N_a}{\partial z} & 0 & ik_x N_a \end{pmatrix} \tag{10}$$

Where k_x and k_y are the Fourier images of the x and y directions respectively.

Then, rewriting $\mathbf{B}_a$ as: $[\mathbf{B}_a] = [\mathbf{B}_{\boldsymbol{a}}]_1 + ik_x[\mathbf{B}_{\boldsymbol{a}}]_2 + ik_y[\mathbf{B}_{\boldsymbol{a}}]_3$

$$[\mathbf{B}_a]_1 = \begin{pmatrix} 0 & 0 & 0 \\ 0 & 0 & 0 \\ 0 & 0 & \frac{\partial N_a}{\partial z} \\ 0 & 0 & 0 \\ 0 & \frac{\partial N_a}{\partial z} & 0 \\ \frac{\partial N_a}{\partial z} & 0 & 0 \end{pmatrix} [\mathbf{B}_a]_2 = \begin{pmatrix} N_a & 0 & 0 \\ 0 & 0 & 0 \\ 0 & 0 & 0 \\ 0 & N_a & 0 \\ 0 & 0 & 0 \\ 0 & 0 & N_a \end{pmatrix} [\mathbf{B}_a]_3 = \begin{pmatrix} 0 & 0 & 0 \\ 0 & N_a & 0 \\ 0 & 0 & 0 \\ N_a & 0 & 0 \\ 0 & 0 & N_a \\ 0 & 0 & 0 \end{pmatrix} \tag{11}$$

The wave equation for the thin-layer system is simplified and expressed in the frequency-wavenumber domain as $([\mathbf{K}] - \omega^2[\mathbf{M}])\mathbf{U} = \mathbf{P}$, where $\mathbf{U}$ and $\mathbf{P}$ are displacements and tractions, respectively, and $\mathbf{M}$ is the corresponding mass matrix. $\mathbf{K}$ is the global stiffness matrix:

$$[\mathbf{K}] = [\mathbf{K}_0] + ik_x[\mathbf{K}_1] + ik_y[\mathbf{K}_2] + k_x^2[\mathbf{K}_3] + k_y^2[\mathbf{K}_4] + k_x k_y[\mathbf{K}_5] \tag{12}$$

Where:

$$[\mathbf{K}_0] = \int_0^h [\mathbf{B}_1]^T [\mathbf{D}] [\mathbf{B}_1] |J| d\xi \tag{13}$$

$$[\mathbf{K}_1] = \int_0^h [\mathbf{B}_1]^T [\mathbf{D}] [\mathbf{B}_2] |J| d\xi - \int_0^h [\mathbf{B}_2]^T [\mathbf{D}] [\mathbf{B}_1] |J| d\xi \tag{14}$$

$$[\mathbf{K}_2] = \int_0^h [\mathbf{B}_1]^T [\mathbf{D}] [\mathbf{B}_3] |J| d\xi - \int_0^h [\mathbf{B}_3]^T [\mathbf{D}] [\mathbf{B}_1] |J| d\xi \tag{15}$$

$$[\mathbf{K}_3] = \int_0^h [\mathbf{B}_2]^T [\mathbf{D}] [\mathbf{B}_2] |J| d\xi \tag{16}$$

$$[\mathbf{K}_4] = \int_0^h [\mathbf{B}_3]^T [\mathbf{D}] [\mathbf{B}_3] |J| d\xi \tag{17}$$

ACCEPTED MANUSCRIPT

$$[\mathbf{K}_5] = \int_0^h [\mathbf{B}_2]^T [\mathbf{D}] [\mathbf{B}_3] |J| d\xi + \int_0^h [\mathbf{B}_3]^T [\mathbf{D}] [\mathbf{B}_2] |J| d\xi \quad (18)$$

Also, $|J|$ is the determinant of the Jacobian matrix and $\mathbf{D}$ is the constitutive matrix, in which elastic and isotropic material properties are used in this paper (Bian et al. 2011).

This classic thin-layer formulation gives the response of a medium with a fixed rigid base, however an infinitely deep soil is required for the majority of critical velocity problems. To overcome this, a variety of absorbing boundary formulations have been proposed (Kausel 1986)(Barbosa et al. 2012). In this work, Thompson-Haskell matrices are formed in a similar manner to the previous derivation and appended to those above. The size of each matrix is $3(n+1) \times 3(n+1)$ to account for the displacements in vertical, horizontal and longitudinal directions at the half-space interface.

2.2.2 Equivalent stiffness formulation

After the equivalent stiffness is computed in the frequency-wavenumber domain using Equation 3, the system of equations in Equation 1 and 2 are then solved to obtain the displacements of the track components.

Then, scaled Green's function $R(k_x, k_y, \omega)$ can be represented as:

$$R(k_x, k_y, \omega) = (L(k_x, \omega) C_{tg}) \tau^g(k_x, k_y, \omega) \quad (19)$$

Where $\tau^g(k_x, k_y, \omega)$ is the displacement/strain/stress Green's function; $L(k_x, \omega) C_{tg}$ represents the load function, in which $L(k_x, \omega)$ is computed by multiplication of the equivalent stiffness and lower track displacement. Also, C_{tg} is given in Equation 4 and Equation 5.

Inverting the scaled Green's function in the transversal and longitudinal directions using the inverse Fourier transform gives the ground responses in the time-space domain:

$$R(x, y, t) = \frac{1}{(2\pi)^3} \int_{-\infty}^{\infty} \int_{-\infty}^{\infty} \int_{-\infty}^{\infty} R(k_x, k_y, \omega)\, e^{i(\omega t - k_x x - k_y y)} dk_x dk_y d\omega \quad (20)$$

Finally, it is worth noting that because the TLM model is computed in the wavenumber-frequency domain, the moving load effect is taken into account using the shift property of the Fourier transform that allows frequency to be related to wavenumber, i.e., $\omega = \Omega - k_x c$, where Ω is the excitation frequency (set to 0Hz in this work) , k_x is the wavenumber in the direction of moving load, and c is the moving load velocity.

3. Model validation

The model is validated against three test cases which are a combination of numerical and experimental results. Firstly, its ability to model soil improvement below a railway track is verified. Next its output is compared against numerical results from published literature, and finally it is validated against experimental results from a railway line in Portugal (Alves Costa et al. 2012)(Correia dos Santos et al. 2016).

3.1 Soil replacement validation

One advantage of using the TLM for soil modelling is that it is computationally efficient compared to 3D FE analysis. However, one limitation compared to 3D approaches is that all horizontal layers are

ACCEPTED MANUSCRIPT

infinitely long/wide. This is acceptable for many problems because the soil layers below and near the track can be assumed to be horizontal and infinite. However, when considering soil replacement/improvement, to minimise cost, remediation is typically only performed directly below the track. The TLM cannot capture this localised improvement and instead assumes the improvement is infinite rather than just below the track.

To determine the effect of this assumption on the ability of the proposed model to simulate soil replacement, 3D FE tests are performed using ABAQUS. The 3D track consists of rail, railpad, slab and sub-ballast components. The track is fully coupled to a 3D soil model with x,y,z dimensions: 50*32*12m; which utilises infinite element absorbing boundaries in the free-field to reduce artificial reflections. Two soils, with constant density, 2000kg/m^3, are considered and shown in Figure 5:

1. In real-life, when considering soil replacement, it is likely that due to the practicalities of construction the sides of the replacement zone would be sloped (dashed grey lines in Figure 5). However, for validation the improved area is considered to have vertical sides (solid grey lines in Figure 5). This is the worst-case scenario and thus most likely to challenge the limitations of the model. The Young's modulus of the improved soil is 150MPa, while the Young's modulus of the non-remediated soil is set to 45MPa. Considering that soil improvement can be undertaken to an arbitrary depth, and that it is the vertical improvement edges likely to introduce errors, the soil improvement is considered for the full model depth.
2. A fully homogenous soil with properties: 150MPa. This represents the TLM approximation of post-soil improvement where the improvement was performed to the infinite horizontal layers

To compare the results generated by both models, track receptance is considered. Figure 6 (left) shows the results for all frequencies are similar. A small discrepancy is seen at low frequency which is governed by the static stiffness of the overall track-ground model, however the difference is negligible. This is because wave energy first propagates from the track into the soil directly below the track (i.e. where remediation is located). Then, when it spreads from this region, for the case of the remediated soil it moves through a stiff to soft soil interface thus not generating significant reflection. Similarly, in the homogenous TLM assumption, it also does not experience a reflection, thus making the approximations similar. Further, Figure 6 (right) compares the track displacement time history for a train running close to the critical velocity (550km/h) for both cases. It is seen that again the response is similar, with a small discrepancy in the peak value. Therefore, considering the validation is for the most challenging test case (i.e. case of a vertical replacement barrier) it can be concluded that the proposed model is capable of accurately modelling the effects of soil replacement.

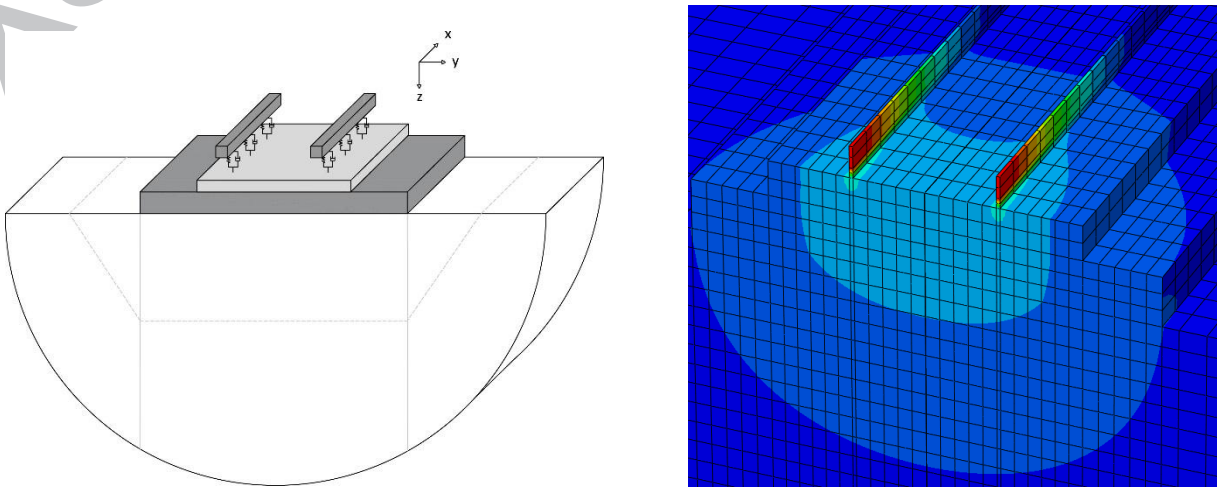

Figure 5: Left: Layout of soil replacement geometry, Right: Cut through ABAQUSs model showing track and soil response during receptance test

ACCEPTED MANUSCRIPT

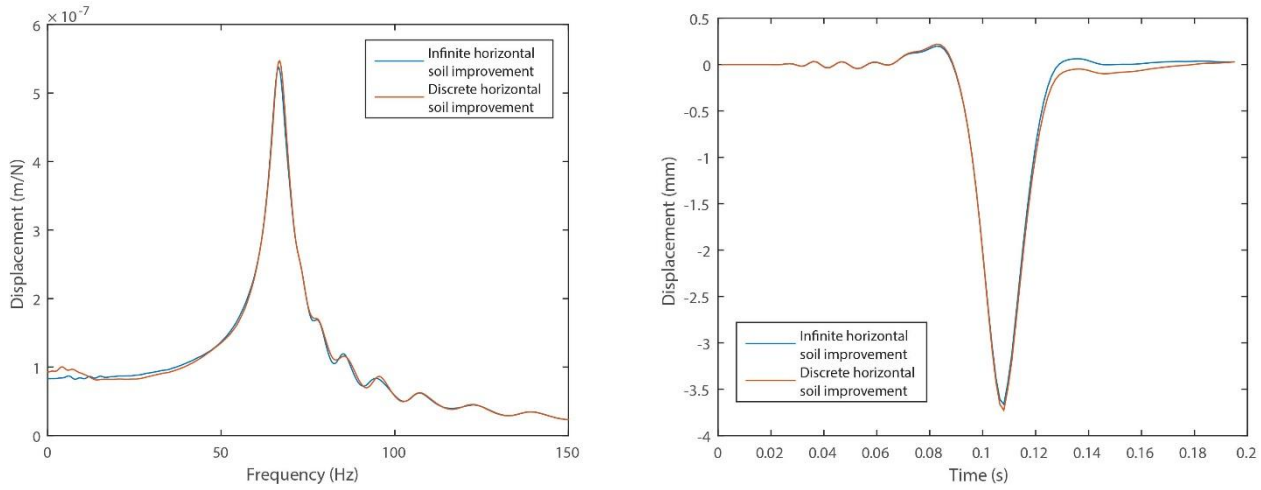

Figure 6: Comparison between simplified and detailed soil replacement geometry (Left: static rail receptance excitation, Right: moving load excitation time history)

3.2 Numerical validation

A numerical comparison is made against an alternative, peer-reviewed and validated track-ground railway model (Kaynia et al. 2000). Like all models though, the peer-reviewed approach was originally found to have discrepancies between its results and field data (Kaynia et al. 2000). Therefore, it is intended for a qualitative comparison.

Figure 7 illustrates the modelling scenario, for which a combined track/embankment structure rests on a multi-layered soil. Also, the soil is composed of 5 layers, with the lowest layer being infinitely deep, as described in Table 1. However, it should be noted that to account for non-linear soil behaviour (i.e. stiffness degradation with strain), the soil properties in the previous (Kaynia et al., 2000) study are manually changed to account for this. Therefore, to ensure consistency between validations, the same 'degraded' properties are used for comparison (i.e. the track/embankment has a bending rigidity EI of $80\ \mathrm{MN/m^2}$ when the train speed is either 185 km/h or 200 km/h, and $200\ \mathrm{MN/m^2}$ when the train speed is 70 km/h). It is worth noting that the bending stiffness is updated by changing the Young's modulus E, instead of changing the dimensions of the embankment. Train loading is chosen to replicate an X2000 train running in two directions (Northbound and Southbound), at speeds of 70, 185 and 200km/h (Figure 8).

ACCEPTED MANUSCRIPT

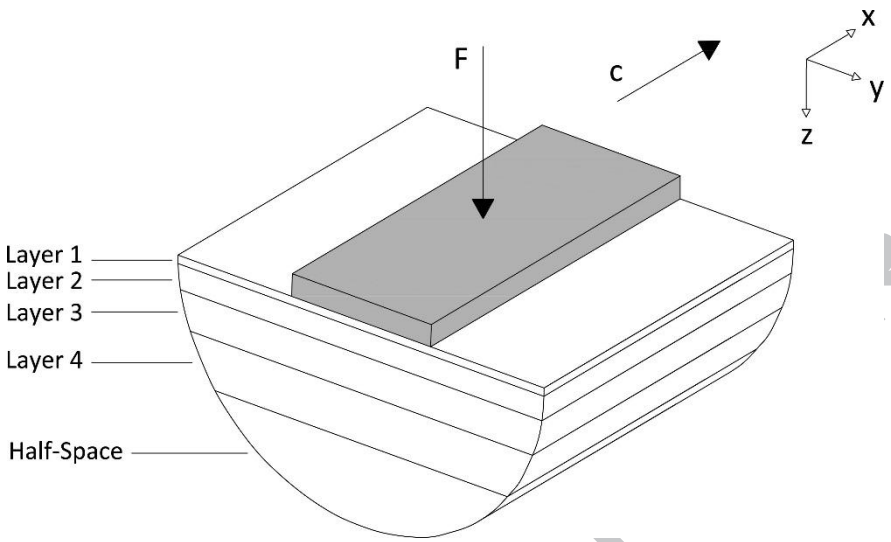

Figure 7: Schematic representation of track-ground interaction model

ACCEPTED MANUSCRIPT

ACCEPTED MANUSCRIPT

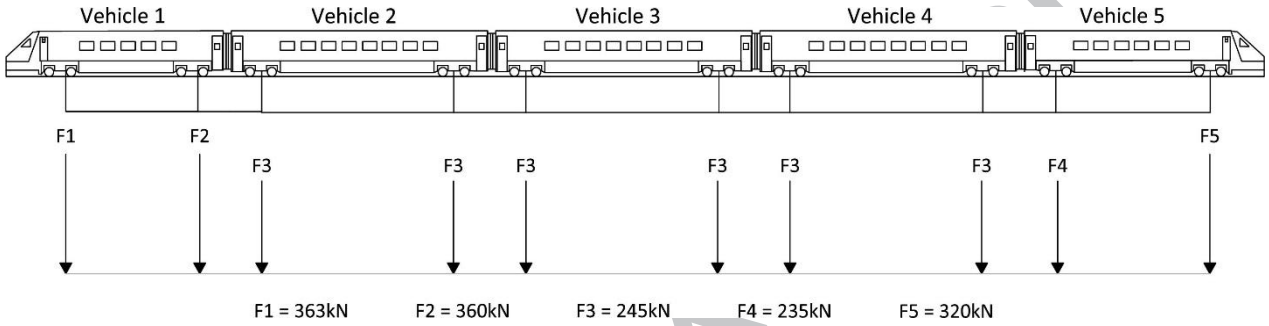

Figure 8: Train loads applied in the numerical simulation

Table 1: Soil properties used in the simulation for train velocity of 70 km/h and 200 km/h

Soil layer	Layer thickness (m)	Density (kg/m^3)	Young's modulus (MPa)		Poisson ratio		Damping	
			c = 70	c ≥ 185	c = 70	c ≥ 185	c = 70	c ≥ 185
Crust	1.1	1500	23	19	0.49	0.49	0.04	0.063
Organic clay	3	1260	6	4	0.5	0.5	0.02	0.058
Clay 1	4.5	1475	19	16	0.5	0.5	0.05	0.098
Clay 2	6	1475	33	32	0.5	0.5	0.05	0.064
Half-space	---	1475	44	44	0.5	0.5	0.05	0.06

Table 2: Velocity and direction of the compared simulation cases

	Case 1	Case 2	Case3
Velocity (km/h)	70 km/h	185 km/h	200 km/h
Direction	Southbound	Northbound	Southbound

ACCEPTED MANUSCRIPT

Figure 9 shows the rail displacement time history comparison between the published result and the solution calculated using the proposed model. In this example, the velocity is lower (70 km/h) than the critical speed, meaning the response is relatively quasi-static. This is representative of a soft-soil site, where although significant wave propagation is not occurring (i.e. the train speed is not close to the critical velocity), track displacements are still high. It is seen that the new model is a strong match to the published data.

Figure 10 shows the second validation, at the higher speed of 185km/h in the Northbound direction. On this occasion the train speed is closer to the critical velocity meaning dynamic wave propagation is significantly more prominent than at 70km/h. This results in amplified displacements, in both the upward and downward directions, particularly for the leading and trailing wheels. Again the model is able to accurately predict track response. The discrepancy at higher frequencies is partly due to having to approximate the published time histories because raw time history data was unavailable.

Finally, Figure *11* shows the comparison between the proposed model and the published results at a speed of 200km/h. Again the speed is close to the critical velocity and the dynamic effects are dominant. However, compared to the speed of 185km/h, the displacements associated with the leading and trailing wheels have reduced, while the response due to the central wheels has increased. Again, the model predicted this accurately. Therefore is it concluded that the model is accurate and any discrepancies between models are as likely to be from the published result as from the proposed model. Also, it should be stated that the track-ground coupling in the model presented by (Kaynia et al. 2000) is slightly different from the presented approach, since hybrid time-frequency domain is adopted in the former.

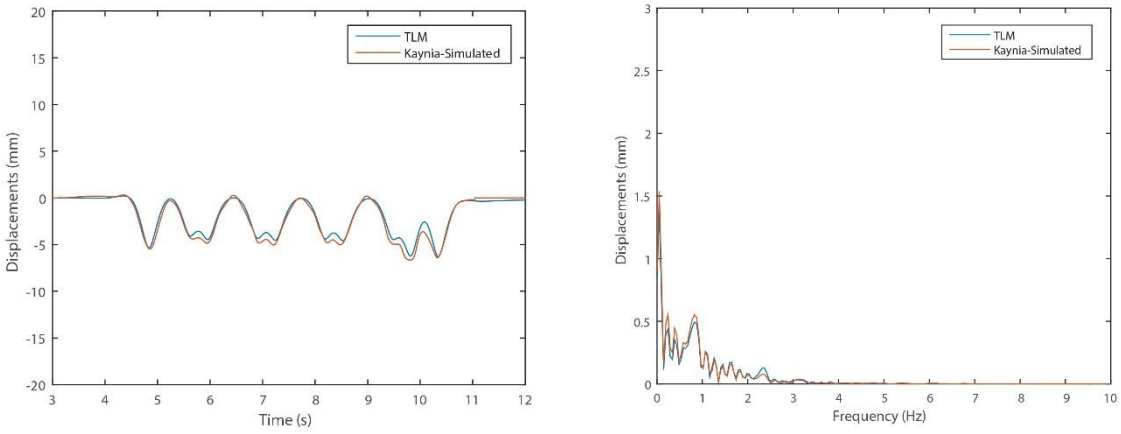

Figure 9: Track displacement for Southbound train at 70 km/h (case 1) in time domain (Left) and frequency domain (Right)

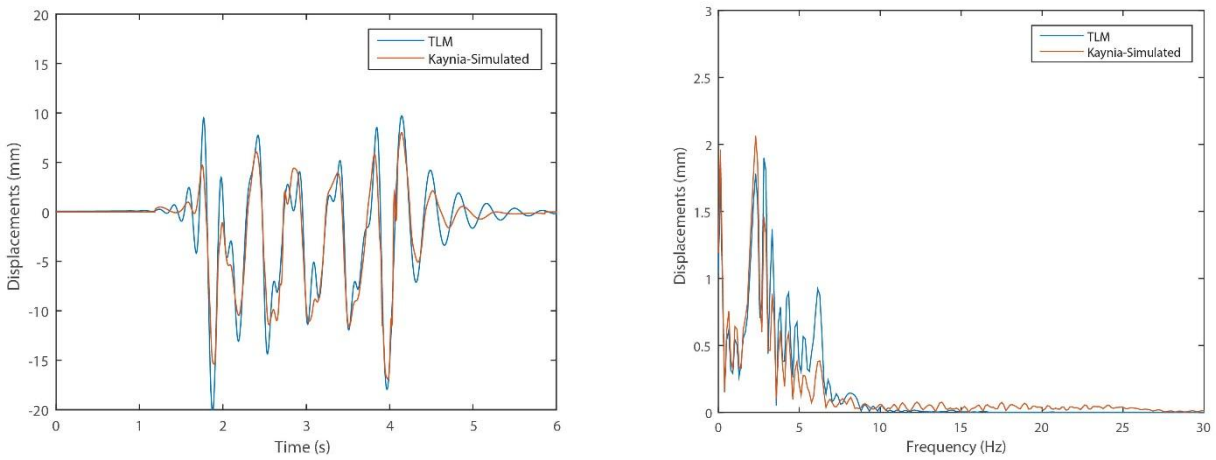

ACCEPTED MANUSCRIPT

Figure 10*: Track displacement for Northbound train at 185 km/h (case 2) in time domain (Left) and frequency domain (Right)*

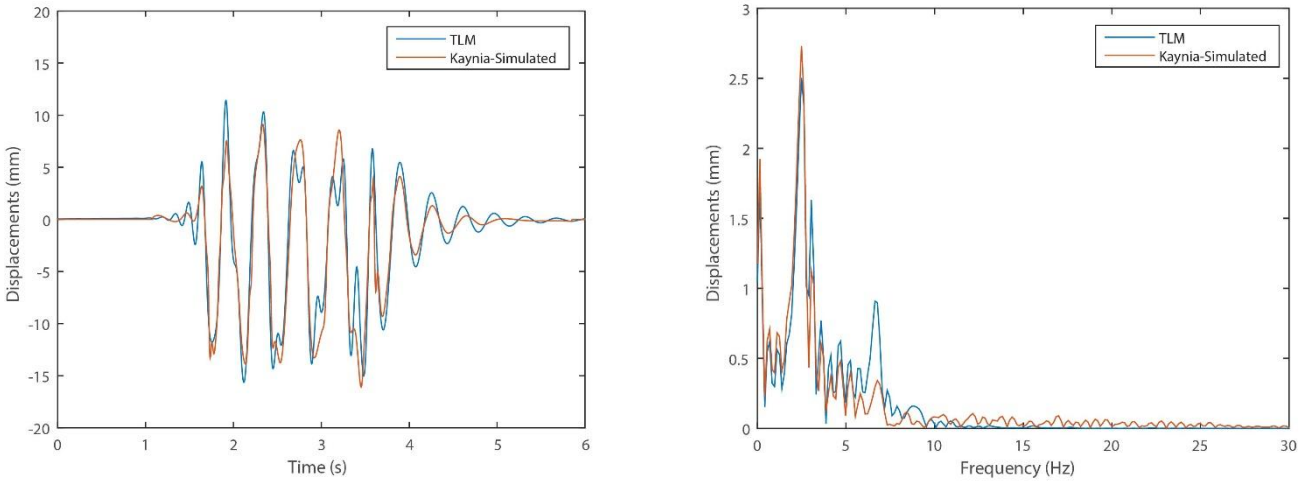

Figure 11*: Track displacement for Southbound train at 200 km/h (case 3) in time domain (Left) and frequency domain (Right)*

3.3 Experimental validation

In addition to numerical validation, an experimental validation is performed against data from a railway line in western Portugal, near the town of Carregado. At this site, a comprehensive series of tests were used to assess the soil characteristics, track properties and the system response due to the passage of Alfa-Pendular trains (Alves Costa et al. 2012).

The train is composed of 6 vehicles, with the geometry and axle loads shown in Figure 12. Regarding the geometric settings of the model, there are 10 soil layers supported by bedrock, and ballast and sub-ballast lay on top of the uppermost soil layer. The height of the ballast is 0.57m, the Young's modulus 97MPa, the Poisson ratio 0.12 and the density 1590 kg/m^3. The same parameters but for the sub-ballast are 0.55m, 212MPa, 0.2 and 1910 kg/m^3, respectively. One difference between the track described in Equation 1 and that at Carregado, is the presence of a sub-ballast layer below the ballast. To account for this change, the analytical track equation is modified as shown in Equation 21, where E_{sb}, C_{psb}, h_{sb}, u_{sb} are the Young's modulus, compression wave speed, thickness and displacement of the sub-ballast, respectively.

ACCEPTED MANUSCRIPT

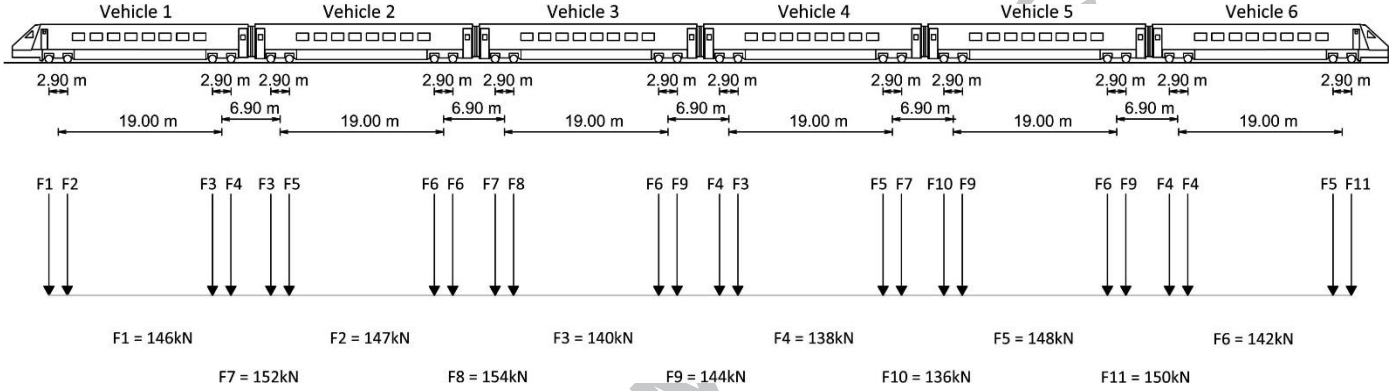

Figure 12: Geometry and mechanical properties of the Alfa-Pendular train

$$\begin{bmatrix} EIk_x^4 + k_p - \omega^2 m_r & -k_p & 0 & 0 \\ -k_p & k_p + \dfrac{2\omega E_b b\alpha}{tg\left(\dfrac{\omega}{C_{pb}} h_b\right) C_{pb}} - \omega^2 m_s & -\dfrac{2\omega E_b b\alpha}{\sin\left(\dfrac{\omega}{C_{pb}} h_b\right) C_{pb}} & 0 \\ 0 & -\dfrac{2\omega E_b b\alpha}{\sin\left(\dfrac{\omega}{C_{pb}} h_b\right) C_{pb}} & \dfrac{2\omega E_b b\alpha}{tg\left(\dfrac{\omega}{C_{pb}} h_b\right) C_{pb}} + \dfrac{2\omega E_{sb} b\alpha}{tg\left(\dfrac{\omega}{C_{psb}} h_{sb}\right) C_{psb}} & -\dfrac{2\omega E_{sb} b\alpha}{\sin\left(\dfrac{\omega}{C_{psb}} h_{sb}\right) C_{psb}} \\ 0 & 0 & -\dfrac{2\omega E_{sb} b\alpha}{\sin\left(\dfrac{\omega}{C_{psb}} h_{sb}\right) C_{psb}} & \dfrac{2\omega E_{sb} b\alpha}{tg\left(\dfrac{\omega}{C_{psb}} h_{sb}\right) C_{psb}} + k_{eq} \end{bmatrix} \times \begin{Bmatrix} \widetilde{u_r}(k_x, \omega) \\ \widetilde{u_s}(k_x, \omega) \\ \widetilde{u_b}(k_x, \omega) \\ \widetilde{u_{sb}}(k_x, \omega) \end{Bmatrix} = \begin{Bmatrix} \tilde{P}(k_x, \omega) \\ 0 \\ 0 \\ 0 \end{Bmatrix} \quad (21)$$

ACCEPTED MANUSCRIPT

Figure 13 (Left) compares the simulated rail displacement and the field measurement in the time domain. Further, Figure 13 (Right) shows the corresponding frequency content comparison. It is seen that there is a strong match between the predicted and measured values. Regarding the time history, the correlation is strong for both the magnitude and timing of response. Regarding the frequency content, the key dominant frequencies and their harmonics are accurately simulated. Any small discrepancies at high frequencies are likely to have been due to wheel-rail irregularities, or to any other dynamic excitation mechanisms, which were ignored during prediction, since only quasi-static excitation is taken into account.

Figure 14 (Left) shows the sleeper velocity during train passage and Figure 14 (Right) shows the corresponding frequency content. Again the agreement is strong for both cases.

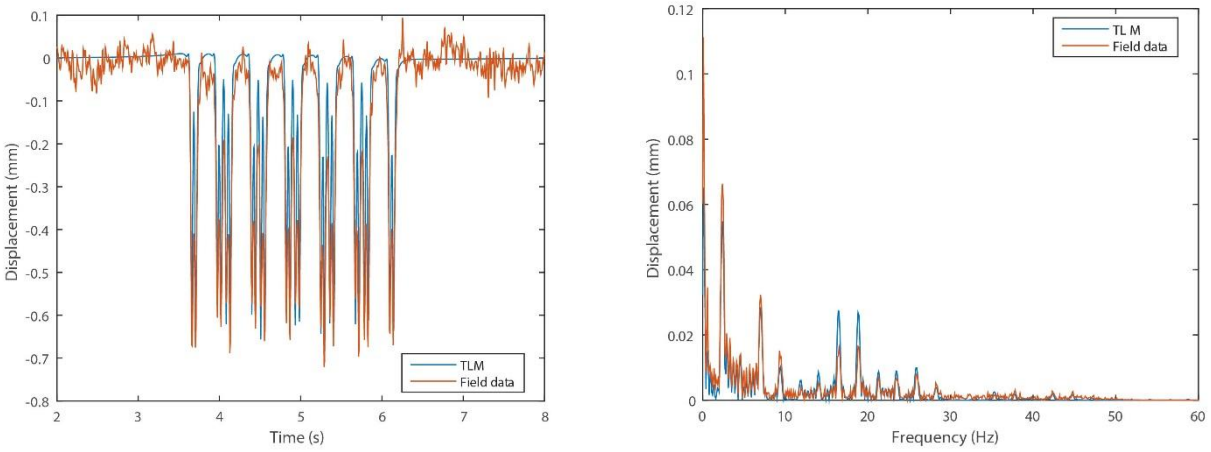

Figure 13: Rail displacement due to the train passage in both time content (Left) and in frequency content (Right)

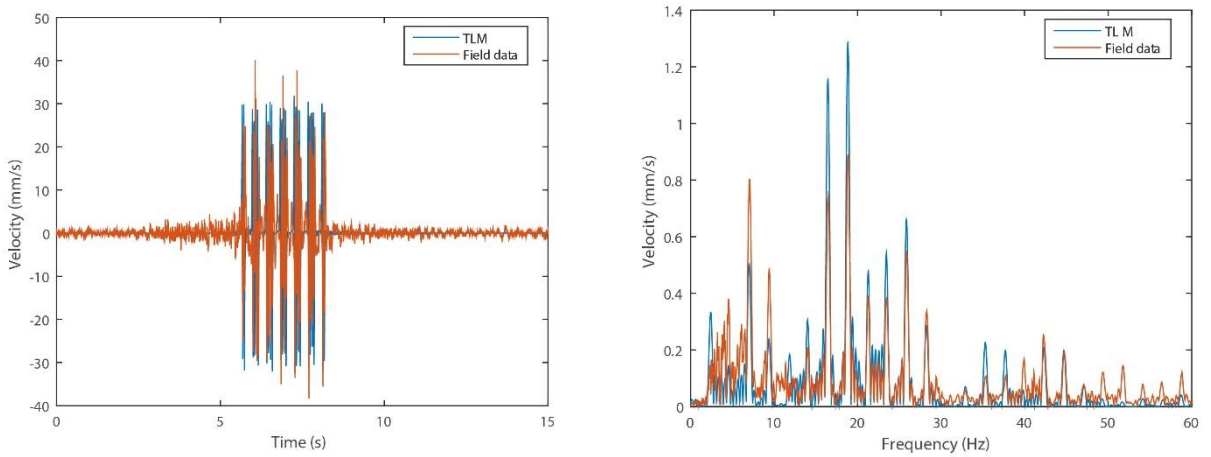

Figure 14: Vertical sleeper velocity due to the train passage in both time content (Left) and in frequency content (Right)

4. Soil replacement strategies

On railway lines, areas of low stiffness ground can be remediated using a variety of techniques, including soil replacement and soil improvement. These techniques are expensive, particularly as depth of remediation increases, meaning it is desirable to optimise/minimise improvement depth. This is challenging to determine because at high train speeds, the low frequency wave energy generated penetrates deep into the underlying soil. This can be solved using the model because its thin-layer formulation makes it well suited for analysing the effect of soil replacement and soil improvement.

ACCEPTED MANUSCRIPT

To show the capabilities of the model, three soil test cases are undertaken to determine the effect of improvement depth and stiffness for both ballasted and slab tracks. They are chosen to represent scenarios that could be encountered at soft soil sites and have the properties outlined in Table 3:

1. A homogenous low stiffness soil
2. A low stiffness soil overlying a stiffer soil
3. A low stiffness soil sandwiched below a stiff embankment and above a stiffer underlying soil

Regarding soil improvement, for each of the three cases, the soft soil is improved to a maximum depth of 5m, considering the effect of five cumulative 1m thick improvements. All improvements are considered as a homogeneous horizontal layer and the track displacement is analysed for each. Further, for case 1, three different stiffness' of improvement are considered. The train loading is a single 18 tonne axle load moving at 330 km/h, which is considered as the maximum operational speed for new high speed rail lines in UK, for all three study cases. The ballasted and slab track properties are shown in Table 4.

Table 3: Soil properties

	Layer thickness (m)	Young's modulus (MPa)	Poisson's ratio	Density (kg/m^3)	Damping
Soil 1	[∞]	[45MPa]	0.35	1800	0.03
Soil 2	[5 ∞]	[45MPa 120MPa]	0.35	1800	0.03
Soil 3	[2 5 ∞]	[200MPa 45MPa 120MPa]	0.35	1800	0.03

Table 4: Track properties (ballasted track and slab track)

		Ballasted track	Slab track
Rail	EI_r (Nm^2)	1.26×10^7	1.26×10^7
	m_r (kg/m)	120	120
Railpad	k_p (N/m)	5.5×10^8	5.5×10^8
	c_p (Ns/m)	2.5×10^5	2.5×10^5
Sleepers	m_s (kg/m)	490	-
Ballast/Slab	$h_{ballast/slab}$ (m)	0.35	0.35
	$E_{ballast/slab}$ (MPa)	150	3×10^4
	$2b$ (m)	2.5	2.5
	ρ (kg/m^3)	1600	2500

4.1 Soil case 1

Soil test case 1 consists of a homogenous, infinitely deep soil with a stiffness of 45MPa. Five different depths of soil improvement from the soil–track interface are considered (1, 2, 3, 4, 5m), and for each, three different magnitudes of stiffness improvement are tested (150, 200, 250MPa).

Figure 15 shows the effect on rail displacement due to these changes for both ballasted and slab tracks, with the results further summarised in Table 5. As expected, all displacements for the ballasted track are greater than those for the concrete slab. Considering the ballasted track, all depths of improvement result in reduced displacements, however adding additional improvement at large depth below the ground has less of an effect than at the surface (e.g. adding 1m of improvement to the natural soil provides a greater percentage of reduction compared to adding 1m at a depth of 4m). This is because the Rayleigh wave energy is confined close to the soil surface.

ACCEPTED MANUSCRIPT

Considering the slab track, the performance benefits are less clear, with 1m of improvement (at 150 and 200MPa stiffness's) resulting in increased track deflections. This can be explained by analysing the relationship between train speed and rail deflections, (i.e. the dynamic amplification factor). Figure 16 shows this relationship for the cases of no soil improvement and 1m of improvement. It is seen that the train speed is marginally past the critical velocity when no improvement is performed. However, improving the ground stiffness shifts the critical velocity to a higher speed meaning that the 1m improvement cases are located closer to the peak, resulting in greater displacement amplification. Other than these cases, track displacements are lower than the non-improved case for all improvement depths and stiffness's. Again, the relationship between depth of improvement and rail displacements is non-linear.

Regarding the effect of the stiffness of the replacement soil, as expected, stiffer soils result in lower track deflections. For example, for the ballasted 1m replacement case, the rail displacements are 2.71mm and 2.35mm when the replacement stiffness is 150 and 250MPa respectively. Comparing this to the 2m case, 2m of 150MPa soil has a rail displacement of 1.97mm, meaning the use of 2m of softer fill provides better performance than 1m of stiffer fill. Alternatively though, at greater depths the opposite is true, for example with 4m of stiffer fill providing lower deflections than 5m of softer fill. Also, for the ballasted track, the displacement reduction between 150, 200 and 250MPa is relative constant for all depths of improvement. However, for the slab track this not true, with the percentage benefit between 150MPa and 250MPa at 1m, lower than that for the 5m case. Therefore, considering the non-linear relationships between improved soil stiffness and improvement depth, soil remediation must be undertaken carefully to ensure displacement tolerances are met and cost is minimised.

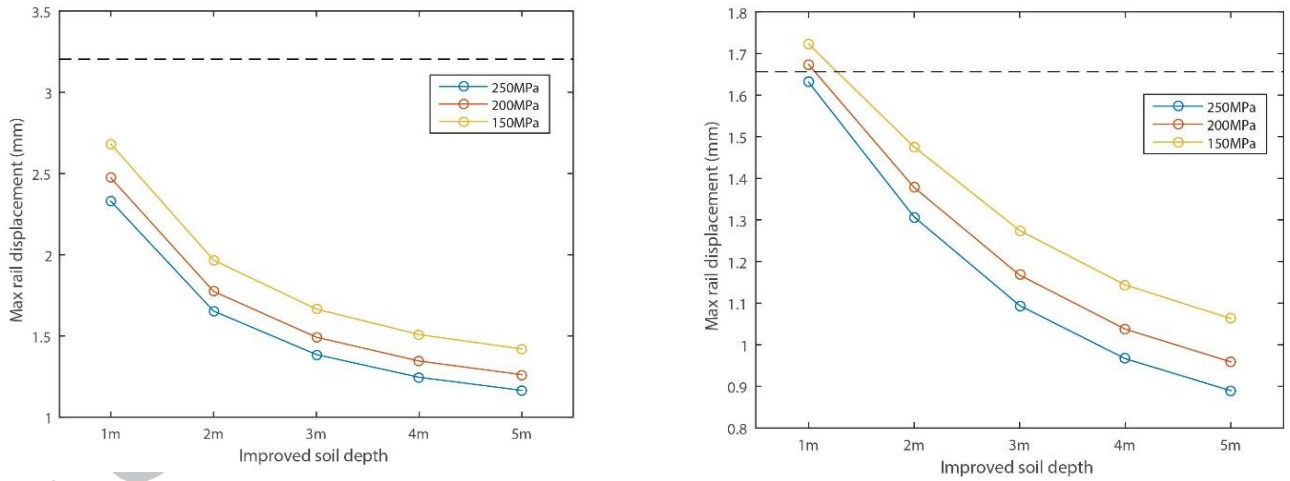

Figure 15: Maximum vertical rail displacement for Soil 1. (Left) Ballasted track; (Right) Slab track; Dashed black line represents the original value

ACCEPTED MANUSCRIPT

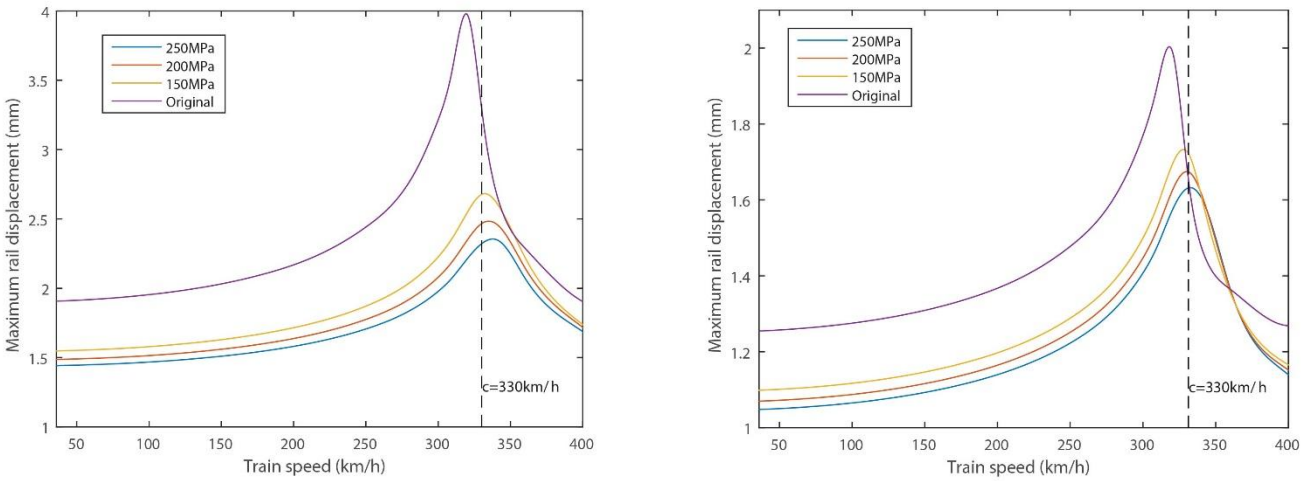

Figure 16: Maximum vertical rail displacement vs train speed, for Soil 1 with 1m of soil replacement. (Left) Ballasted track; (Right) Slab track; Dashed black line represents train speed

Table 5: Rail displacement improvement in percentage terms for Soil 1 at a train speed of 330km/h

Improvement depth	150MPa		200MPa		250MPa	
	Ballasted	Slab	Ballasted	Slab	Ballasted	Slab
1m	16.3%	-4.0%	22.8%	-1.1%	27.3%	1.5%
2m	38.6%	10.9%	44.6%	16.8%	48.3%	21.1%
3m	48.1%	23.1%	53.4%	29.5%	56.7%	33.9%
4m	52.9%	30.9%	58.0%	37.3%	61.1%	41.6%
5m	55.7%	35.8%	60.6%	42.1%	63.6%	46.3%

Additionally, Figure 17 shows a stress time history comparison at the surface of the soil below the central line of the ballasted track, for speeds 20m/s and 92m/s. It is observed that the shape of the stress time histories for low speed is regular but oscillations occur as it approaches the critical velocity. Comparing the maximum stress values at different speeds, the x and y stress components increase by 423% and 448% respectively, while the xz shear stress increases by 371%. In comparison, although the maximum z stress component remains the largest, it only increases by 124% due to the speed change. Therefore at low speed the response is dominated by the vertical response, while at critical speed the entire stress field becomes important.

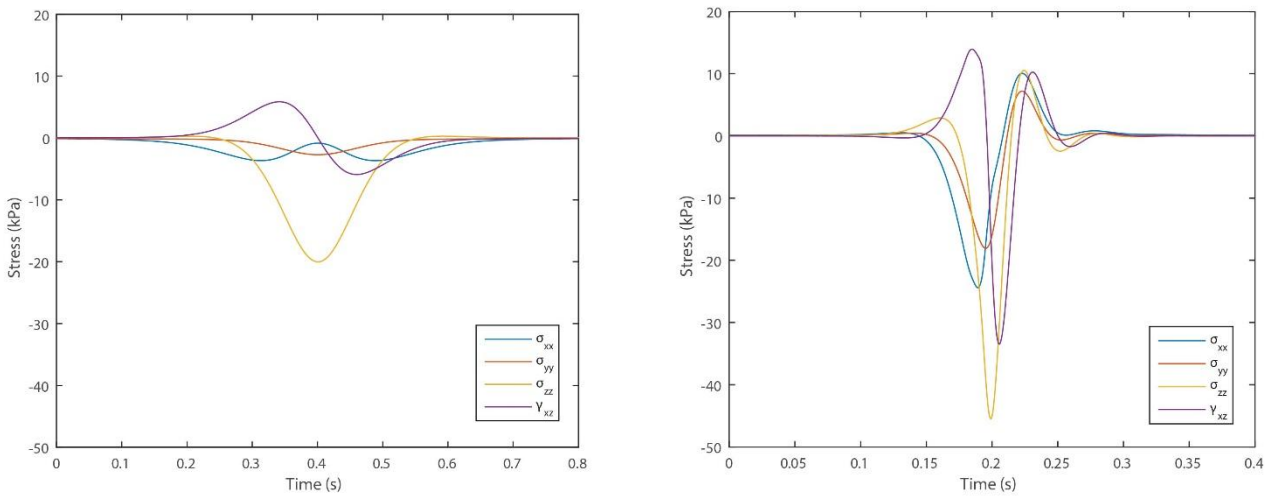

ACCEPTED MANUSCRIPT

Figure 17: Stress time history comparison at the surface for ballasted track. (Left) c=20m/s (Right) c=92m/s

4.2 Soil case 2

Soil test case 2 consists of a 5m deep soft layer (45MPa) overlying a stiffer layer (120MPa), which is homogenous, and infinitely deep. Five different depths of soil improvement from the soil–track interface are considered (1, 2, 3, 4, 5m), where 5m means all of the soft 45MPa layer is replaced. For each case, the soft layer is replaced with a soil of stiffness of 250MPa, and the effect on rail displacement is analysed. Figure 18 shows the effect of soil replacement for both ballasted and slab track cases, with the percentage terms shown in Table 6. Again the concrete slab track has lower deflections due to its elevated bending stiffness, however in contrast to soil case 1, all depths of improvement result in reduced track deflections. For the ballasted track the relationship between improvement depth and rail displacement is highly non-linear. When 1m of improvement is performed, displacements reduce by 49.1%, however the reductions are only 64.4, 69.4, 71.8 and 73.2% for 2, 3, 4, 5m replacements respectively. Therefore for this case, depending upon the desired deflection levels, it may be most cost effective to remediate only the top 1m of soil. For the slab track the relationship is also non-linear, however less pronounced. Again, increasing improvement depth reduces deflections, however the change in performance benefit reduces as the improvement depth approaches 5m.

Figure 19 shows the effect of soil replacement on displacements. It is seen that the unmodified soil gives rise to significant wave propagation, with 'Mach cone' type contours present. In comparison, for the fully remediated soil stratum, the response is more symmetric in both horizontal directions.

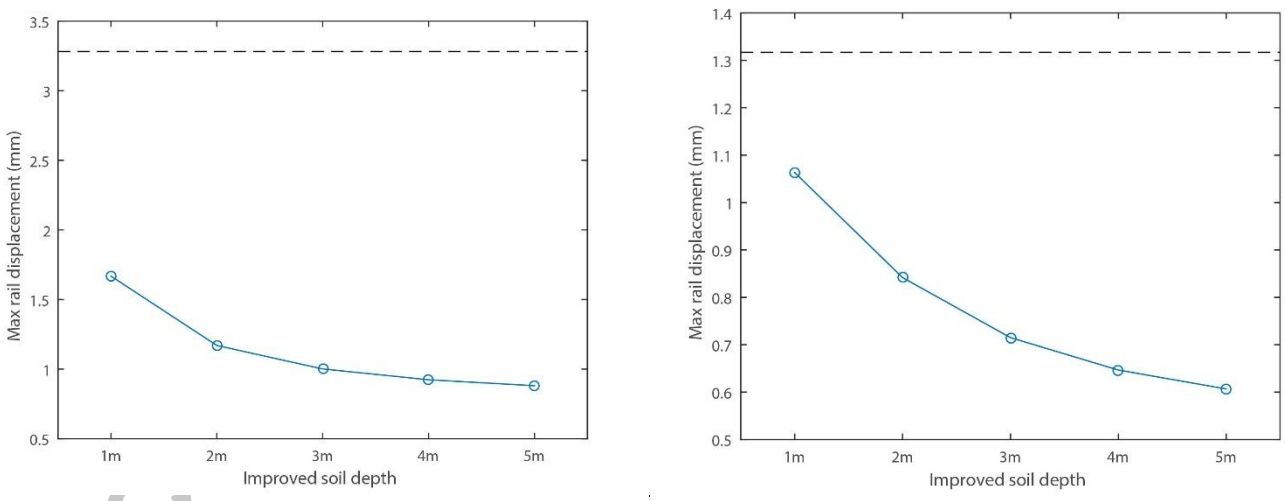

Figure 18: Maximum vertical rail displacement for Soil 2. (Left) Ballasted track; (Right) Slab track; Dashed black line represents the original value

ACCEPTED MANUSCRIPT

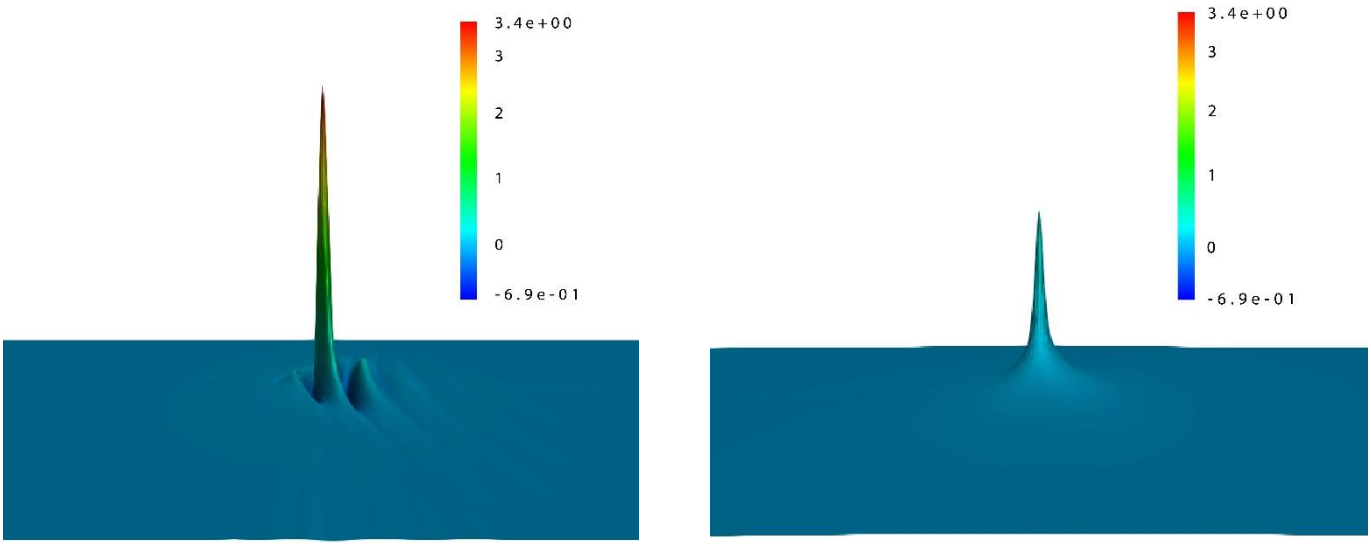

Figure 19: Rail displacement comparisons for Soil 2. (Left) Original soil; (Right) 5m depth of improvement

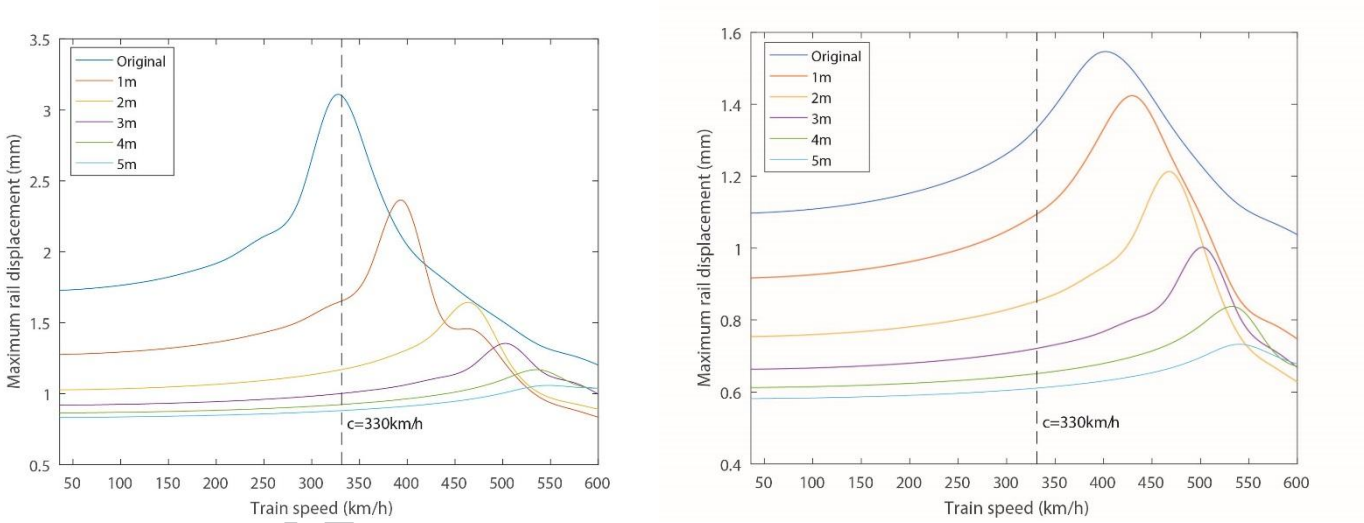

Figure 20: Maximum vertical rail displacement vs train speed, for Soil 2 with different depths of soil replacement strategies. (Left) Ballasted track; (Right) Slab track

Table 6: Rail displacement improvement in percentage for Soil 2 at a train speed of 330 km/h

Improvement depth	250MPa	
	Ballasted	Slab
1m	49.1%	19.3%
2m	64.4%	36.1%
3m	69.4%	45.7%
4m	71.8%	50.9%
5m	73.2%	53.9%

4.3 Soil case 3

Soil test case 3 is chosen to determine the effect of an embankment ((Kouroussis et al. 2016)(Oliver et al. 2016)) overlying a soft soil site. Therefore it consists of a 2m high embankment overlying the soft-stiff

ACCEPTED MANUSCRIPT

stratum from soil case 2 (Figure 21). The embankment is modelled in a simplified manner, i.e., considering it as an additional layer, infinitive in the transversal direction. To simulate the presence of an embankment, it is modelled as an additional soil layer, which has been shown to be a reasonable approximation in (Alves Costa, Calçada, et al. 2010). This results in a 5m thick soft layer (45MPa) sandwiched between two stiffer layers. The upper embankment layer has a stiffness of 200MPa and the lower ground layer is infinitely deep with a stiffness of 120MPa. Again, improvement depths between 1-5m are considered.

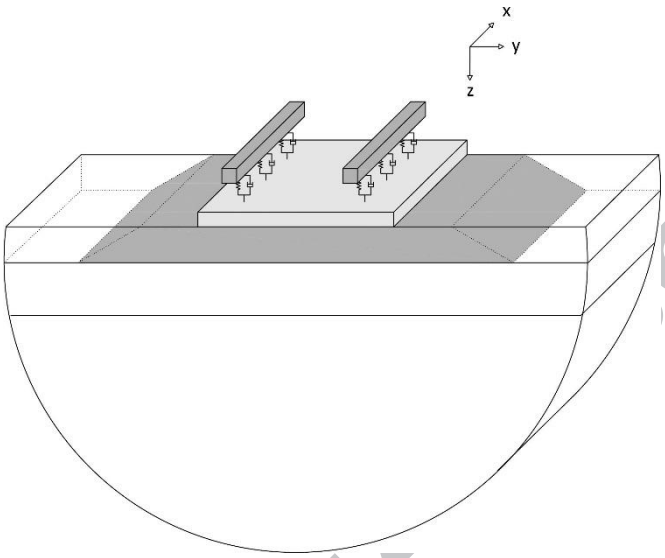

Figure 21: Schematic diagram of the slab track used in the simulation overlaying on the soil

Figure 22 shows the relationship between soil replacement depth and track displacement. It is observed that the stiff embankment causes a significant reduction in rail displacement compared to Figure 18. This is because the dispersion characteristics are shifted the critical velocity to a higher value, due to the presence of the embankment. Similar to soil case 2, all improvement depths result in reduced track displacements, however the relationship is no longer relatively linear. Instead, only a small reduction is achieved by improving 2m compared to 1m, while improving 3m compared to 2m results in a large reduction. This is true for both track types, but more pronounced for the ballasted case. Therefore, depending on the desired rail deflection tolerances, it might be most efficient to replace the top 3m rather than either 2 or 4m. It should also be noted that although the rail displacements for this particular track-soil combination may not have require remediation in practise, the finding of non-linearity in soil improvement depth is also applicable to other track-soil stiffness combinations.

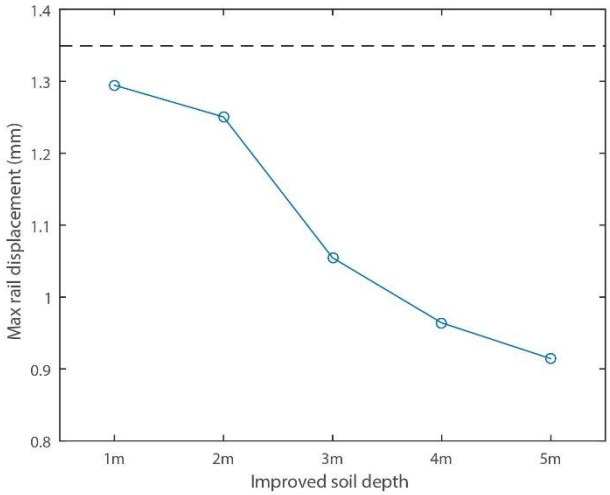

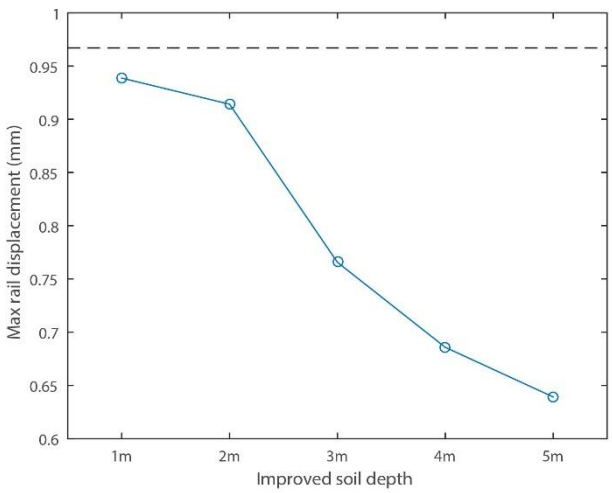

ACCEPTED MANUSCRIPT

Figure 22: Maximum downward rail displacement for Soil 3. (Left) Ballasted track; (Right) Slab track; Dashed black line represents the original value

Table 7: Rail displacement improvement in percentage for Soil 3 at 300 km/h

Improvement depth	250MPa	
	Ballasted	Slab
1m	4.0%	2.9%
2m	7.3%	5.5%
3m	21.8%	20.8%
4m	28.5%	29.1%
5m	32.2%	33.9%

In addition to rail displacements, Figure 23 shows the resulting maximum vertical stresses within the embankment (2m) and soil to a depth of 5m below the embankment. It is seen that despite the soil replacement having a significant impact of rail deflections, the effect on stress levels is less defined. This is particularly true for the ballasted track, however for the slab track, although the stresses for stiffer soils are lower at 7m compared to the softer soils, the upper 2m of the stiffer soil experiences slightly higher stress levels.

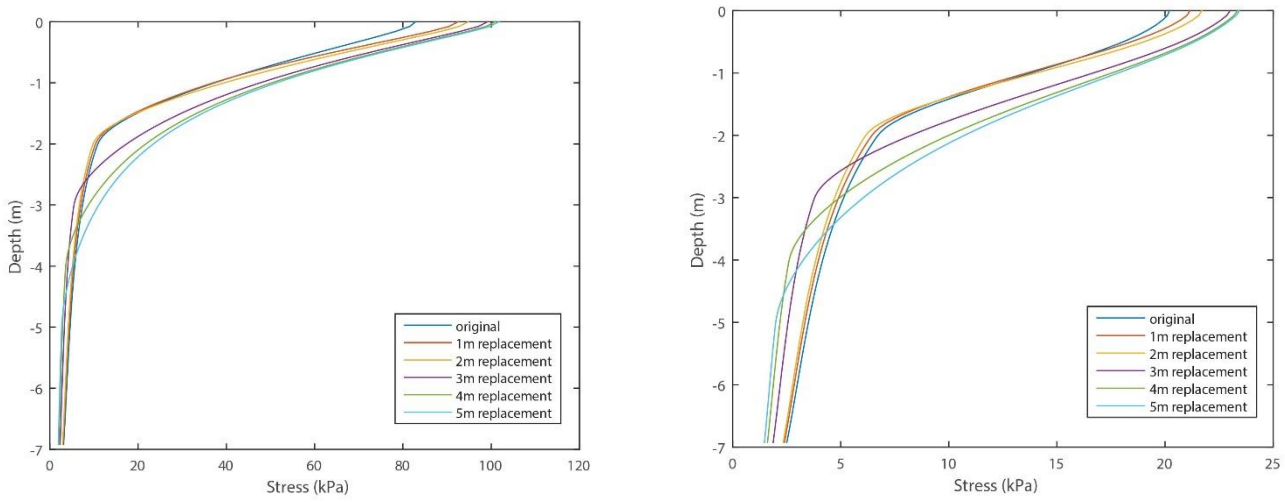

Figure 23: Vertical stress vs Depth for Soil case 3. (Left) Ballasted track; (Right) Slab track

5. Discussion

When planning, designing and constructing a new railway line it is important to assess the track-soil dynamics along the route. If the operational train speed is greater than 50% of the combined track-soil wave speed then there is the potential for dynamic effects to cause excessive track deflections. To mitigate this risk, at the planning stage, a scoping exercise can be performed to approximate the absolute critical velocity. This can be done for example using dispersion curve analysis based upon historical geotechnical data or surface wave testing data. If the train speed is calculated to be greater than 50% of the critical velocity then the TLM model can be used to perform a more detailed assessment (i.e. calculation of track-ground DAF curves). Finally, if soil replacement is deemed necessary then model can be combined with a costing tool to optimise the depth of remediation required, with respect to price.

ACCEPTED MANUSCRIPT

Lastly, it should be noted that the aforementioned analysis assumes linear soil behaviour. As train speeds approach the critical velocity, strain levels within the soil can move to the high strain range (Alves Costa, Calçada, et al. 2010). This results in a non-linear relationship between strain and stiffness. The thin-layer method approach used within the model is well suited to the simulation of these effects.

6. Conclusion

Soil replacement or improvement is commonly used on new railway lines to increase track stiffness, however is expensive. Therefore a model was developed capable of rapidly assessing the effect of different soil improvement depths and stiffness' on track behaviour. The model can therefore be used to optimise soil replacement with respect to construction cost. The modelling methodology comprised of a thin-layer method ground model, coupled in the wavenumber-frequency domain to an analytical track model. It was capable of simulating the deep wave propagation that occurs when approaching critical velocity. Validation was performed using a combination of field experimental data and published numerical results, and the model found to have strong accuracy. To show the model capabilities, three earthwork situations were considered: a homogenous soft soil, a soft soil over a stiff soil, and a stiff embankment resting on a soft soil over a stiff soil. It was found that due to the complex nature of the 3D wave propagation and its dependency on multiple variables, the relationship between improvement depth and rail displacement can be highly non-linear. Therefore soil improvement must be designed carefully to achieve the desired track performance.

7. Acknowledgements

Model development was a collaboration between the University of Porto, Heriot-Watt University and the University of Leeds. The authors would like to thank the Leverhulme Trust (UK), the University of Porto, Heriot Watt University and the University of Leeds. Without their support, this research would not have been possible.

8. Reference

Alves Costa, P., Calcada, R., et al., 2010. A 2.5D finite element model for simulation of unbounded domains under dynamic loading. *Numerical methods in Geotechnical Engineering*, pp.397–404.

Alves Costa, P. et al., 2015. Critical speed of railway tracks. Detailed and simplified approaches. *Transportation Geotechnics*, 2, pp.30–46. Available at: http://dx.doi.org/10.1016/j.trgeo.2014.09.003.

Alves Costa, P., Calçada, R., et al., 2010. Influence of soil non-linearity on the dynamic response of high-speed railway tracks. *Soil Dynamics and Earthquake Engineering*, 30(4), pp.221–235.

Alves Costa, P., 2011. *Vibrações Do Sistema Via-Maciço Induzidas Por Tráfego Ferroviário . Modelação Numérica E Validação Experimental*.

Alves Costa, P., Calçada, R. & Silva Cardoso, A., 2012. Track-ground vibrations induced by railway traffic: In-situ measurements and validation of a 2.5D FEM-BEM model. *Soil Dynamics and Earthquake Engineering*, 32(1), pp.111–128.

Arlaud, E., Costa D'Aguiar, S. & Balmes, E., 2016. Receptance of railway tracks at low frequency: Numerical and experimental approaches. *Transportation Geotechnics*, 9, pp.1–16. Available at: http://dx.doi.org/10.1016/j.trgeo.2016.06.003.

ACCEPTED MANUSCRIPT

Arlaud, E., Costa D'Aguiar, S. & Balmes, E., 2015. Validation of a reduced model of railway track allowing long 3D dynamic calculation of train-track interaction. *Computer Methods and Recent Advances in Geomechanics - Proceedings of the 14th Int. Conference of International Association for Computer Methods and Recent Advances in Geomechanics, IACMAG 2014*, (September), pp.1193–1198. Available at: http://www.scopus.com/inward/record.url?eid=2-s2.0-84907340860&partnerID=tZOtx3y1.

Auersch, L., 2005. The excitation of ground vibration by rail traffic: Theory of vehicle-track-soil interaction and measurements on high-speed lines. *Journal of Sound and Vibration*, 284(1–2), pp.103–132.

Barbosa, J.M. de O., Park, J. & Kausel, E., 2012. Perfectly matched layers in the thin layer method. *Computer Methods in Applied Mechanics and Engineering*, 217–220(October), pp.262–274. Available at: http://dx.doi.org/10.1016/j.cma.2011.12.006.

Bian, X. et al., 2016. Numerical analysis of soil vibrations due to trains moving at critical speed. *Acta Geotechnica*, 11(2), pp.281–294. Available at: http://dx.doi.org/10.1007/s11440-014-0323-2.

Bian, X.. et al., 2011. A 2.5D finite element approach for predicting ground vibrations generated by vertical track irregularities. *Journal of Zhejiang University-SCIENCE A*, 12(12), pp.885–894. Available at: http://link.springer.com/10.1631/jzus.A11GT012.

Bian, X.., Chen, Y.. & Hu, T., 2008. Numerical simulation of high-speed train induced ground vibrations using 2.5D finite element approach. *Science in China Series G: Physics Mechanics and Astronomy*, 51(6), pp.632–650.

Bian, X. & Chen, Y., 2006. An explicit time domain solution for ground stratum response to harmonic moving load. *Acta Mechanica Sinica/Lixue Xuebao*, 22(5), pp.469–478.

Chebli, H., Othman, R., et al., 2008. 3D periodic BE-FE model for various transportation structures interacting with soil. *Computers and Geotechnics*, 35(1), pp.22–32.

Chebli, H., Clouteau, D. & Schmitt, L., 2008. Dynamic response of high-speed ballasted railway tracks: 3D periodic model and in situ measurements. *Soil Dynamics and Earthquake Engineering*, 28(2), pp.118–131.

Connolly, D., Giannopoulos, A., Fan, W., et al., 2013. Optimising low acoustic impedance back-fill material wave barrier dimensions to shield structures from ground borne high speed rail vibrations. *Construction and Building Materials*, 44, pp.557–564.

Connolly, D., Giannopoulos, A. & Forde, M.C., 2013. Numerical modelling of ground borne vibrations from high speed rail lines on embankments. *Soil Dynamics and Earthquake Engineering*, 46, pp.13–19. Available at: http://dx.doi.org/10.1016/j.soildyn.2012.12.003.

Correia dos Santos, N. et al., 2016. Experimental analysis of track-ground vibrations on a stretch of the Portuguese railway network. *Soil Dynamics and Earthquake Engineering*, 90, pp.358–380. Available at: http://dx.doi.org/10.1016/j.soildyn.2016.09.003.

Dieterman, H. a. & Metrikine, a. V., 1996. The equivalent stiffness of a half-space interacting with a beam. Critical velocities of moving load along the beam. *European Journal of Mechanics A/Solids*, 15, pp.67–90.

Ferreira, P.A. & López-Pita, A., 2015. Numerical modelling of high speed train/track system for the reduction of vibration levels and maintenance needs of railway tracks. *Construction and Building Materials*, 79, pp.14–21. Available at: http://dx.doi.org/10.1016/j.conbuildmat.2014.12.124.

François, S. et al., 2010. A 2.5D coupled FE-BE methodology for the dynamic interaction between longitudinally invariant structures and a layered halfspace. *Computer Methods in Applied Mechanics*

ACCEPTED MANUSCRIPT

and Engineering, 199(23–24), pp.1536–1548. Available at: http://dx.doi.org/10.1016/j.cma.2010.01.001.

Fryba, L., 1972. *Vibration of Soilds and Structures under Moving Loads*, Springer Netherlands.

Galvín, P. et al., 2010. A 2.5D coupled FE-BE methodology for the prediction of railway induced vibrations. *Soil Dynamics and Earthquake Engineering*, 30, pp.1500–1512.

Galvín, P. & Domínguez, J., 2007. Analysis of ground motion due to moving surface loads induced by high-speed trains. *Engineering Analysis with Boundary Elements*, 31(11), pp.931–941.

Hall, L., 2003. Simulations and analyses of train-induced ground vibrations in finite element models. *Soil Dynamics and Earthquake Engineering*, 23(5), pp.403–413.

Hendry, M., Hughes, D.A. & Barbour, L., 2010. Track displacement and energy loss in a railway embankment. *Proceedings of the Institution of Civil Engineers - Geotechnical Engineering*, 163(1), pp.3–12. Available at: http://www.icevirtuallibrary.com/doi/10.1680/geng.2010.163.1.3.

El Kacimi, A. et al., 2013. Time domain 3D finite element modelling of train-induced vibration at high speed. *Computers and Structures*, 118, pp.66–73. Available at: http://dx.doi.org/10.1016/j.compstruc.2012.07.011.

Kausel, E., 1981. *An explicit solution for the Green functions for dynamic loads in layered media*,

Kausel, E., 1994. Thin-layer method: Formulation in the time domain. *International Journal for Numerical Methods in Engineering*, 37(6), pp.927–941.

Kausel, E., 1986. Wave propagation in anisotropic layered media. *International Journal for Numerical Methods in Engineering*, 23(8), pp.1567–1578.

Kausel, E. & Roesset, J.M., 1981. Stiffness matrices for layered soils. *Bulletin of the Seismological Society of America*, 71(6), pp.1743–1761.

Kaynia, A.M., Madshus, C. & Zackrisson, P., 2000. Ground vibration from high-speed trains: Prediction and countermeasure. *Journal of Geotechnical and Geoenvironmental Engineering*, 126(Igvc), pp.531–537.

Kouroussis, G. et al., 2011. Discrete modelling of vertical track-soil coupling for vehicle-track dynamics. *Soil Dynamics and Earthquake Engineering*, 31(12), pp.1711–1723. Available at: http://dx.doi.org/10.1016/j.soildyn.2011.07.007.

Kouroussis, G. et al., 2016. Railway cuttings and embankments: Experimental and numerical studies of ground vibration. *Science of the Total Environment*, 557–558, pp.110–122. Available at: http://dx.doi.org/10.1016/j.scitotenv.2016.03.016.

Krylov, V. V., 1995. Generation of ground vibrations by superfast trains. *Applied Acoustics*, 44(2), pp.149–164.

Lamb, H., 1904. On the propagation of tremors over the surface of an elastic solid. *Philosophical Transactions of the Royal Society of London*, 203, pp.1–42.

Madshus, C. & Kaynia, A.M., 2000. High-Speed Railway Lines on Soft Ground: Dynamic Behaviour At Critical Train Speed. *Journal of Sound and Vibration*, 231(3), pp.689–701. Available at: http://linkinghub.elsevier.com/retrieve/pii/S0022460X99926470.

Mezher, S.B. et al., 2016. Railway critical velocity - Analytical prediction and analysis. *Transportation Geotechnics*, 6(October), pp.84–96.

Montalbán, L. et al., 2015. Analysis of Vibrations Generated By Rail Corrugation in a High Speed Track. ,

ACCEPTED MANUSCRIPT

2015(July), pp.12–16.

O'Brien, J. & Rizos, D.C., 2005. A 3D BEM-FEM methodology for simulation of high speed train induced vibrations. *Soil Dynamics and Earthquake Engineering*, 25(4), pp.289–301.

Oliver, B. et al., 2016. The effect of embankment on high speed rail ground vibrations. *International Journal of Rail Transportation*, 4(4), pp.229–246. Available at: https://doi.org/10.1080/23248378.2016.1220844.

Powrie, W., Yang, L.A. & Clayton, C.R.I., 2007. Stress changes in the ground below ballasted railway track during train passage. *Proceedings of the Institution of Mechanical Engineers, Part F: Journal of Rail and Rapid Transit*, 221(2), pp.247–262.

Sheng, X., Jones, C.J.C. & Thompson, D.J., 2003. A comparison of a theoretical model for quasi-statically and dynamically induced environmental vibration from trains with measurements. *Journal of Sound and Vibration*, 267(3), pp.621–635.

Shih, J.Y., Thompson, D.J. & Zervos, A., 2016. The effect of boundary conditions, model size and damping models in the finite element modelling of a moving load on a track/ground system. *Soil Dynamics and Earthquake Engineering*, 89, pp.12–27. Available at: http://dx.doi.org/10.1016/j.soildyn.2016.07.004.

Shih, J.Y., Thompson, D.J. & Zervos, A., 2017. The influence of soil nonlinear properties on the track/ground vibration induced by trains running on soft ground. *Transportation Geotechnics*, 11, pp.1–16. Available at: http://dx.doi.org/10.1016/j.trgeo.2017.03.001.

Steenbergen, M.J.M.M. & Metrikine, A. V., 2007. The effect of the interface conditions on the dynamic response of a beam on a half-space to a moving load. *European Journal of Mechanics, A/Solids*, 26(1), pp.33–54.

Steenbergen, M.J.M.M., Metrikine, A. V. & Esveld, C., 2007. Assessment of design parameters of a slab track railway system from a dynamic viewpoint. *Journal of Sound and Vibration*, 306(1–2), pp.361–371.

Thompson, D., 2008. *Railway noise and vibration: mechanisms, modelling and means of control*, Elsevier.

Varandas, J.N. et al., 2016. A Numerical Study on the Stress Changes in the Ballast Due to Train Passages. *Procedia Engineering*, 143(Ictg), pp.1169–1176. Available at: http://dx.doi.org/10.1016/j.proeng.2016.06.127.

Yang, Y.B., Hung, H.H. & Chang, D.W., 2003. Train-induced wave propagation in layered soils using finite/infinite element simulation. *Soil Dynamics and Earthquake Engineering*, 23(4), pp.263–278.

Zhai, W., He, Z. & Song, X., 2010. Prediction of high-speed train induced ground vibration based on train-track-ground system model. *Earthquake Engineering and Engineering Vibration*, 9(4), pp.545–554.

ACCEPTED MANUSCRIPT

ACCEPTED MANUSCRIPT

Highlights

1. High track dynamics and critical velocity possible on new high speed rail lines
2. Soil replacement or improvement can be used to improve rail-track dynamics
3. Thin-layer method numerical model shown, capable of optimising improvement depth/stiffness
4. Improvement depth and stiffness shown to have non-linear effect on track/rail displacements
5. Soil replacement or improvement can result in both increases and decreases of displacement

ACCEPTED MANUSCRIPT